Two-Phase, Two-Component Concurrent Flow in Packed Beds," *AIChE J.*, **13**, 1196 (1967).
Uchida, S., and S. Fujita, "Pressure Drop Through Packed Towers," *J. of the Soc. of Chem. Ind. of Japan*, **41**, 275 (1938).
Weekman, V. W., "Heat Transfer and Fluid Flow for Concurrent, Gas-Liquid Flow in Packed Beds," PhD Thesis, Purdue Univ. (1963).
Whitaker, S., "Advances in the Theory of Fluid Motion in Porous Media," *Ind. Eng. Chem.*, **61**, 14 (1969).
Wijffels, J. B., J. Verloop, and F. J. Zuiderweg, "Wetting of Catalyst Particles under Trickle Flow Conditions," *Chemical Reaction Engineering II*, ACS Monograph Ser. No. 133, 151 (1974).

Manuscript received March 18, 1983; revision received October 18, and accepted October 20, 1983.

Development of Improved Bubble Disruption and Dispersion Technique by an Applied Electric Field Method

With the aid of nonuniform DC electric fields, an improved bubble disruption and dispersion technique has been developed for dielectric fluid bubble column reactors. The basic mechanisms which lead to bubble disruption and dispersion in the system have been studied both experimentally and theoretically. The influence of operating variables, liquid properties and electrode geometry on the present applied electric field method has been conducted. The efficiency of power consumption by using the present technique has also been revealed.

SUMITOSHI OGATA and KAZUSHI TAN
Department of Chemical Engineering
Kyushu University
Fukuoka, Japan 812

KIYOTO NISHIJIMA
Department of Electrical Engineering
Fukuoka University
Fukuoka, Japan 814

JEN-SHIH CHANG
Department of Engineering Physics
and
Institute for Energy Studies
McMaster University
Hamilton, Ontario, Canada L8S 4M1

SCOPE

It is well known that bubble column reactors have a wide range of applications in many components of chemical industrial process such as absorption, catalytic slurry reactions, bioreactions, coal liquefaction, etc. These reactors are preferred because of simplicity of operation and low operating costs. Bubble column reactors have recently been reviewed by Mashelkan (1970) and Shah et al. (1982). Main objectives of designing better mass transfer bubble column reactors, other than energy efficiency, are to have better insight of the residence time, the uniformity, and the gas-liquid interfacial area.

In this paper, a new type of bubble dispersion technique based on applied electric field method for a dielectric fluid is introduced, and the basic bubble disruption and dispersion mechanisms as well as system efficiency are investigated both theoretically and experimentally. To understand the uniformity, interfacial area, and residence time, the analysis started with mechanism of bubble disruption and dispersion, and where this process would occur inside the reactors. The numerical analyses of electric field distribution have been conducted with the consideration of existence of bubbles, and compared with experiments at bubble injection point. The influence of operational variables, liquid properties and electrode geometry on the system efficiency has been investigated experimentally and compared with the existing techniques.

S. Ogata was a visiting researcher at the Department of Engineering Physics, McMaster University, in 1981 and is presently at the Ohita University, Japan.
All correspondence concerning this paper should be addressed to J. S Chang.

CONCLUSIONS AND SIGNIFICANCE

The study has been conducte to develop a new technique based on applied electric field method for bubble size reductions and dispersions. The effect of electrical properties of the liquids, the electrode gap and the operational conditions in the present method have been investigated. The results are:

(1) The magnitude of electric pressure can be evaluated from electric field calculation by the charge simulation method. Adequate agreement between the theoretical prediction and the experiment has been obtained.

(2) The efficiency increases with decreasing conductivity of liquids.

(3) The operation at narrower electrode gap and smaller gas flow rate has been observed to provide better system efficiencies in the present range of experiment.

(4) The energy needed for bubble size reductions of nonpolar liquids are extraordinary and lower than those for stirred vessel.

(5) A rising velocity of bubbles are likely accelerated by the electrohydrodynamic (EHD) flow to enhance better bubble dispersions.

This technique has a potential advantage if used in a relatively smaller dielectric constant fluid which is often used in various chemical industries.

INTRODUCTION

The new bubble size reduction and dispersion technique is developed by using electrohydrodynamical force instead of ordinary mechanical forces such as stirred vessel. The principle of this technique is based on size reduction of gas bubbles by a nonuniform electric field and electric field coupled fluid flow.

Zacky et al. (1977) first demonstrated a possibility of size reduction of noble gas bubble by a nonuniform electric field. In this case, an electric pressure was observed at the end of a hypodermic needle by a high applied dc voltage. Ogata et al. (1979, 1980), using similar method and apparatus, studied the bubble size reduction under wide range of experimental conditions. They observed that:

(1) Substantial bubble size reduction was observed, and the effect increases with increasing electric conductivity and/or permittivity.

(2) Due to the increasing electric pressure at the end of the gas injection needle by an applied field, the gas flow rate has been reduced. These phenomena are also observed to depend on the electric properties of liquids.

(3) Due to the reducing electric power loss, the energy efficiency of bubble size reduction increases with decreasing electric conductivity.

(4) The above-mentioned phenomena varied to some extent by changing the polarity of applied voltage. For example, a monodispersed bubble was obtainable by use of dc voltage regardless of its polarities of negative or positive, while employment of ac voltage made them nonuniform.

(5) Existence of corona discharge has been observed at a certain voltage for the liquids with larger permittivity. In this case, the electric pressure started to decrease and, to the contrary, the gas flow rate was recovered.

(6) Generation of an electrohydrodynamic flow was observed during the experiments. They suggested that this field-induced flow possibility affects not only the movement of the bubble, but also the mechanisms of bubble disruption.

Sato et al. (1979) also carried out similar experiments in water and reported remarkable field effects on the bubble size reduction. They also observed the strong effect of spark discharge on the bubble size distribution. Nevertheless, their results confirmed the phenomena observed by Ogata et al. (1979, 1980).

The objective of the present study is to obtain sufficient information on the bubble dispersion phenomenon by using an applied electric field method. The field intensity around the nozzle tip is calculated with the presence of bubbles for various permittivities of liquid. The electric pressure predicted by the above calculations is compared with the experiments. The energy efficiency is obtained in liquids of interest for gas flow rates from 0.4 to 1 mL/s, electrode gap from 1 to 8 cm, applied voltage from 0 to 15 kV, conductivity from 10^{-5} to 10^{-2} S/m, and relative permittivity from 2 to 25.

THEORETICAL ANALYSIS OF BUBBLE DISRUPTION AND DISPERSION MECHANISMS

The behavior of bubble in an electric field is not simple, and several physical processes must be considered. Among these processes, the most important phenomena are the bubble disruption, the electrostatic pressure generation, and the eletrohydrodynamic flow generation due to the existence of electric field.

Bubble Disruption via Bubble Elongation Due to the Applied Electric Field

The process has been analyzed by Garton and Krasucki (1964). The elongation of bubble due to the electric field in a gas-liquid system can be expressed by:

$$E = \left(\frac{\sigma}{\epsilon_o \epsilon_1 r_o}\right)^{1/2} \left\{\frac{\epsilon_1}{\epsilon_1 - \epsilon_2} - G\right\} \left\{\frac{8A^2 B}{3\gamma(\epsilon_1 - \epsilon_2)}\right\}^{1/4} \cosh^{1/2}\theta \quad (1)$$

where

$$3\theta = \cosh^{-1}\left[\frac{Pr_o}{\sigma}\left\{\frac{27\gamma^5}{2(1+\gamma^2)^3}\right\}^{1/2}\right]$$

$$A = 2\gamma - 1 - 1/\gamma^2$$

$$B = 2\epsilon_1\gamma^3 - \epsilon_2(1+\gamma^2)$$

$$G = \frac{1}{\gamma^2 - 1}\left[\frac{\gamma \cosh^{-1}\gamma}{(\gamma^2-1)^{1/2}} - 1\right]$$

Here, γ is the ratio of the major to minor semiaxis, σ is the surface tension, P is the pressure within the bubble, r_o is the radius of bubble without electric field, and ϵ_1 and ϵ_2 are relative permittivities of liquid and gas, respectively. Instability of interface, which leads to bubble disruption, can be obtained from the Kelvin Helmholtz instability analysis (Brunner and Chang, 1980) as follows:

$$(u_g - u_l)^2 F_o + \frac{\sigma}{\rho_1}\frac{\partial^2 \xi}{\partial x^2} - g\xi\left(1 - \frac{\rho_2}{\rho_1}\right) \geq \frac{1}{2\rho_1}(\epsilon_2 - \epsilon_1)\frac{(\epsilon_1 + 2\epsilon_2)}{3\epsilon_2} E_{\text{int}}^2. \quad (2)$$

where ξ is the wave height in gas-liquid interface, u_g and u_l are local gas and liquid velocity, F_o is a constant dependent upon bubble size, g is the gravitational acceleration, E_{int} is the electric field at the interface, ρ_1 and ρ_2 are density of liquid and gas, respectively. The bubble disrupted when ξ equals minor axis of elongated bubble. The numerical value of γ-E characteristics for the present experimental ranges are discussed in Appendix I.

Electrostatic Pressure Head at the Gas Injection Point

According to Kao (1961), the electric pressure working on a bubble surface in a dielectric liquid can be expressed by

$$P_e = \epsilon_2(\epsilon_1/\epsilon_2 + 2)(\epsilon_1/\epsilon_2 - 1)E^2/6. \quad (3)$$

To carry out the electric pressure calculation on the bubble surface at the injection point, we should place another assumption; that is, an averaged field intensity works on the bubble surface as defined by:

$$\overline{E} = \frac{1}{d_B}\int_{L-d_B}^{L} E(z)dz \quad (4)$$

Equation 4 contains an assumption itself that the size of bubbles separating from the end of the nozzle is equal to double that of the nozzle diameter. The numerical values of P_e are discussed and compared with experiments later.

EHD Flow of Liquid Due to the Applied Electric Field

Electrohydrodynamics in a single-phase incompressible laminar flow without space charge can be obtained from the solution of the momentum equation as follows (Apfel'Baum et al. 1978; Chang and Tran, 1981).

$$\rho\frac{\partial \underline{U}}{\partial t} + \rho(\underline{U}\cdot\nabla)\underline{U} = -\nabla P + \mu\nabla^2\underline{U} - \frac{1}{2}\epsilon_o\epsilon\nabla E^2 - \frac{\epsilon_o}{2}E^2\nabla\epsilon \quad (5)$$

If we introduce nondimensional variables $u = U/U_o$, $\psi = E/E_o$, $\tau = tU_o/d$, $R_E = \frac{1}{2}(\epsilon_o\epsilon E_0^2/\rho U_o^2)$, $\tilde{\nabla} = d\nabla$ and $p = P/\rho U_o^2$, with $U_o = \mu/\rho d$, where E_o is the electric field at injection point, Eq. 5 becomes

$$\frac{\partial \underline{u}}{\partial t} + (\underline{u}\cdot\tilde{\nabla})\underline{u} = -\tilde{\nabla}p + \frac{1}{Re}\tilde{\nabla}^2\underline{u} - R_E\{\tilde{\nabla}\psi^2 + \psi^2\tilde{\nabla}\epsilon\} - \underline{g}' \quad (6)$$

Equation 6 shows that the fluid inside the vessel overcome gravity head and starts to move, when $R_E > 1$ and an existence of normalized nonuniform field $\psi = f(r,Z)$. In the two phase flow, an electric field in the gas-liquid interface play an important role in fluid motion, as reported by Brunner and Chang (1980). In this case, the effect may enhance fluid velocity as large as one order of magnitude higher than that of the single-phase flow.

In order to estimate the role played by the above three processes, an electric field around the nozzle tip is calculated by a charge simulation method.

The concept of this calculation method assumes a number of discrete charges (point, ring and rod-like charges) in the conductor (here, it is the nozzle) on which the charge distributes continuously. Thus, distributed real charge would be displaced by assumed charge Q_i ($i = 1, 2, \ldots, N$). The magnitude of Q_i can be determined so that their integrated effect satisfies the boundary conditions exactly at a selected same number of positions on the boundary. Therefore,

$$\sum_{i=1}^{N} P_iQ_i = \phi_c \quad (7)$$

Here, P_i is the potential coefficient associated with Q_i, and ϕ_c is the potential of the conductor. If Q_i is determined from Eq. 7, the potential and field intensity E at point $G(x,y,z)$ can be calculated by Eqs. 8 and 9, respectively, by

$$\phi(s) = \sum_{i=1}^{N} Q_iP_i(\zeta) \quad (8)$$

$$E(s) = \sum_{i=1}^{N} Q_iF_i(\zeta) \quad (9)$$

where $P_i(\zeta)$ and $F_i(\zeta)$ are the potential and field coefficients at location ζ, respectively. The calculated results are shown in Figures 1 and 3. Here, vertical distance z from grounded electrode and electric field E are normalized by an electrode gap L and nominal field intensity $E_0(= V/L)$, respectively.

Figure 1 shows the effect of bubble radius R_2 on the electric field along the center line of the vessel E_z near injection nozzle for ethanol, where $z/L = 1$ is the edge of the injection nozzle (Figure 5). The electric field profile near the leading and trailing edges of the bubbles becomes sharper, Figure 1. Moreover, the magnitude

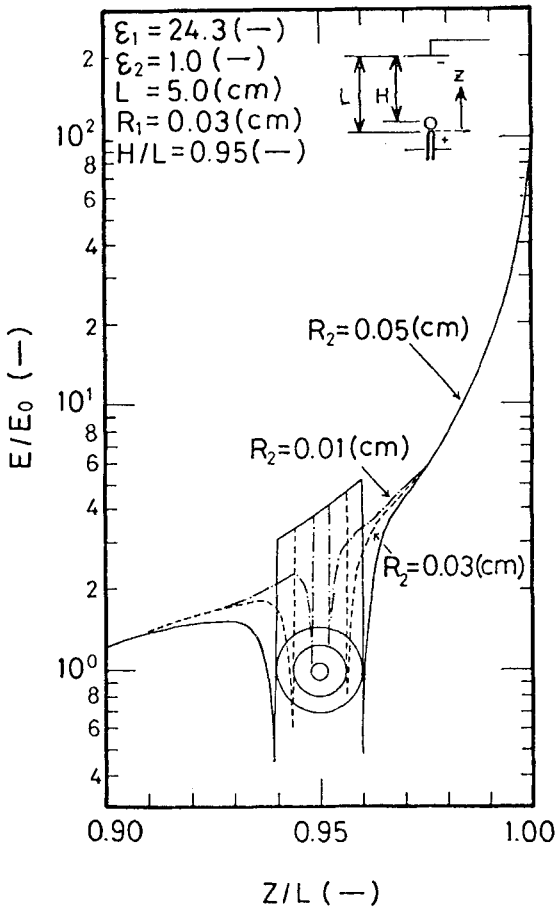

Figure 1. Variations of normalized field intensity E/E_o as a function of normalized vertical distance z/L for various bubble size R_2 for ethanol at electrode gap L = 5 cm.

of field in the bubbles is higher than that of outside. This strong electric field implies that the gas corona discharge can take place inside bubbles as has been experimentally observed by Ogata et al. (1979, 1980) and Sato et al. (1979).

A typical example of observation of corona discharge in the present experiment is shown in Figure 2 for ethanol at 10 kV. The

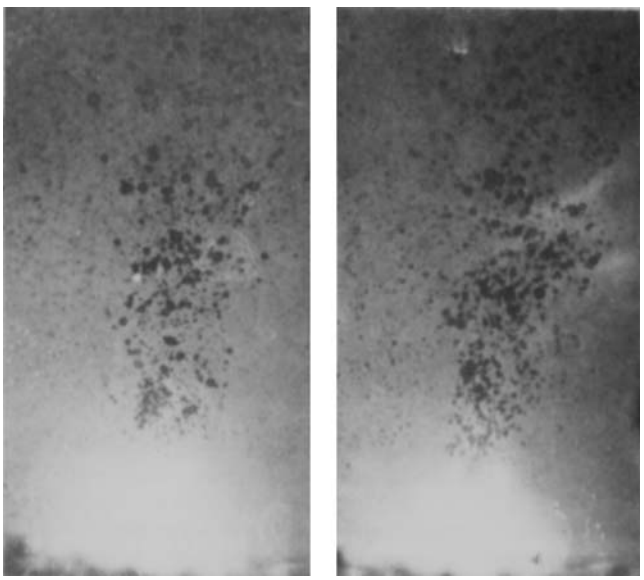

Figuer 2. A typical example of the picture superimposed by corona and bubbles for ethanol at V = 10 kV and M_0 = 0.66 mL/s.

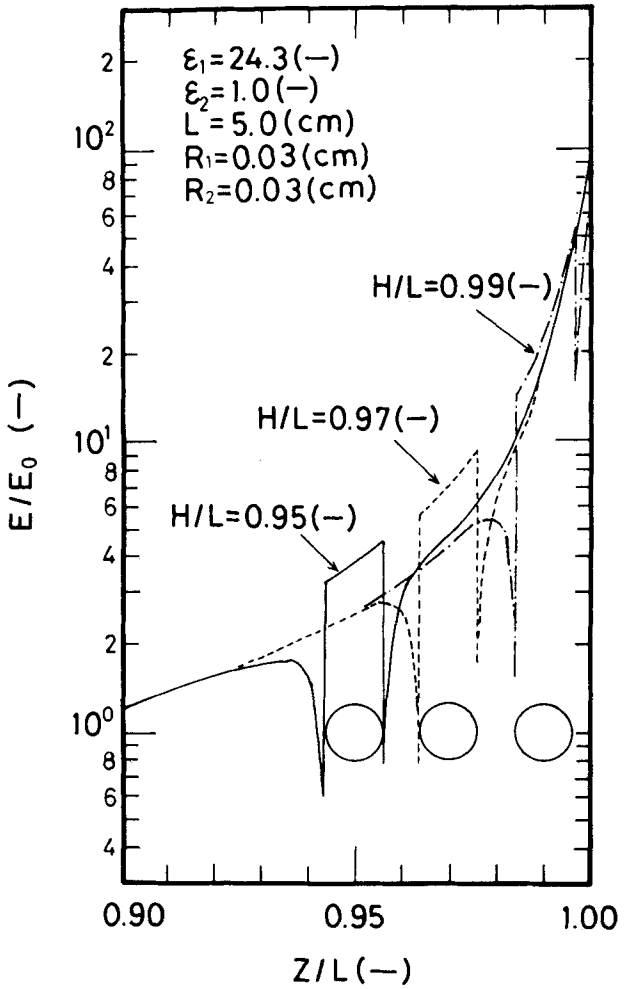

Figure 3. Variations of normalized field intensity E/E_o as a function of normalized vertical distance z/L for various bubble location H for ethanol at L = 5 cm and R_2 = 0.03 cm.

picture is superimposed by discharging corona and a weak back light for taking a shadow graph of bubbles.

The distortion of the field also depends on the locations of bubbles. An example is shown in Figure 3 for ethanol. Figure 3 shows that the difference of field intensities between leading and trailing edges of bubble becomes more pronounced when bubble approaches to the nozzle tip.

Figures 1 and 3, and other calculations also show that the disruption of the bubbles not only occurs at the edge of the injection nozzle, but also may occur as far as half-way between the two electrodes, since the step-up effect of electric field due to the existence of bubbles is still strong enough to elongate the bubbles as far as these locations. Similar conclusions can be obtained for EHD flow, since $R_E > 1$ can be observed at almost any location of the vessel when $V \geq 1$ kV. This implies that the strong EHD flow will be induced in the system with bubble disruptions and bubbles may disperse more efficiently.

From these theoretical predictions, we may conclude that:

(1) In the absence of corona discharge, the efficient bubble disruption and dispersion can be obtained with smaller permittivity and conductivity environment.

(2) Bubble disruption not only occurred near the injection point, but also existed in the wider space inside the vessel.

(3) Strong EHD flow has been predicted when the permittivity of fluid is larger. Therefore, bubbles are more efficiently dispersed inside the vessel.

EXPERIMENTAL APPARATUS AND PROCEDURES

The experimental apparatus used in the present work is shown in Figure 4. The rectangular cross-section (4 × 4 cm), 15 cm tall glass test vessel along with geometrical configuration of electrodes, is shown in Figures 4 and 5.

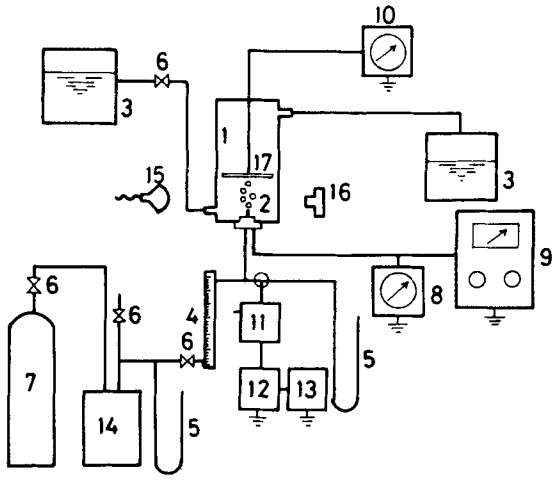

Figure 4. Schematic diagram of experimental apparatus.

The electrical properties of the liquids used in the present experiment are shown in Table 1. Nitrogen gas was injected into liquids, where flowmeter was used for gas flow rate measurement. A stainless steel hypodermic needle was employed as a nozzle. The nozzle's inside and outside diameters were 0.27 and 0.52 cm, respectively. A positive dc voltage was applied to

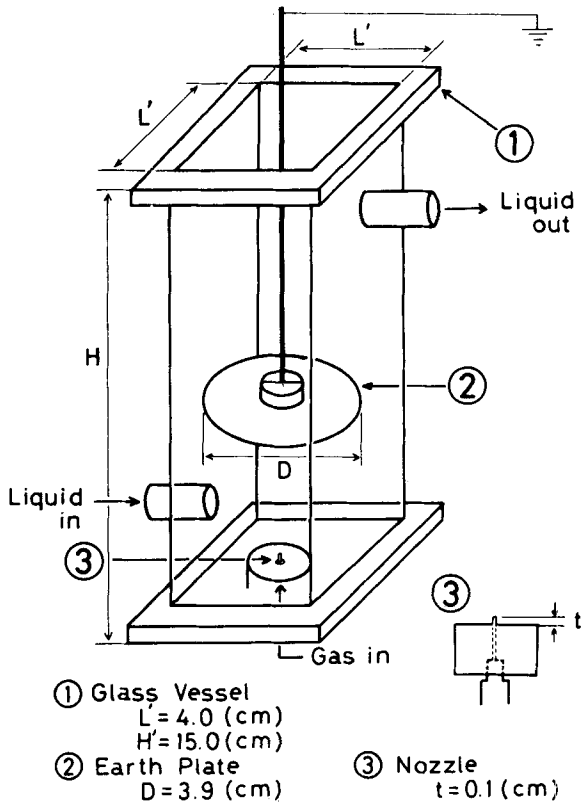

Figure 5. Geometrical configuration of the test vessels and electrodes.

TABLE 1. PHYSICAL PROPERTIES OF LIQUIDS TO BE TESTED (AT 20°C)

	Conductivity (S/m)	Relative Permittivity*
Ethanol	1.0×10^{-5}	24.3
Aniline	9.0×10^{-7}	6.89
Chlorobenzene	2.0×10^{-8}	5.71
Cyclohexane	2.5×10^{-11}	2.2
Kerosine	7.9×10^{-11}	2.1

* Cited from Kagaku Binran (2nd Ed., in Japanese).

the nozzle, while a brass disc electrode was grounded, so that a nonuniform dc field wa formed between the nozzle and the disc. The produced electric pressure was measured by a water manometer. The electric pressure generation processes was observed by a diaphragm-type pressure transducer and displayed in a magnetoscillograph. The superimposed strobo-pictures were taken for the measurements of bubble sizes as well as rising velocity and the Sauter mean diameter was used for the calculations of the energy efficiency.

RESULTS AND DISCUSSION

Electric Pressure at the End of the Nozzle Electrode

As described earlier, electric pressure P_e can be calculated by Eqs. 3 and 4 by using the results of electric field calculations. The experimental results of pressure changes due to the applied voltage are shown in Figures 6 and 7 for various liquids and electrode gaps respectively, where the theoretical predictions described in the previous section are also compared with current results. Figures 6 and 7 show that sufficient agreement between measured and calculated results are obtained.

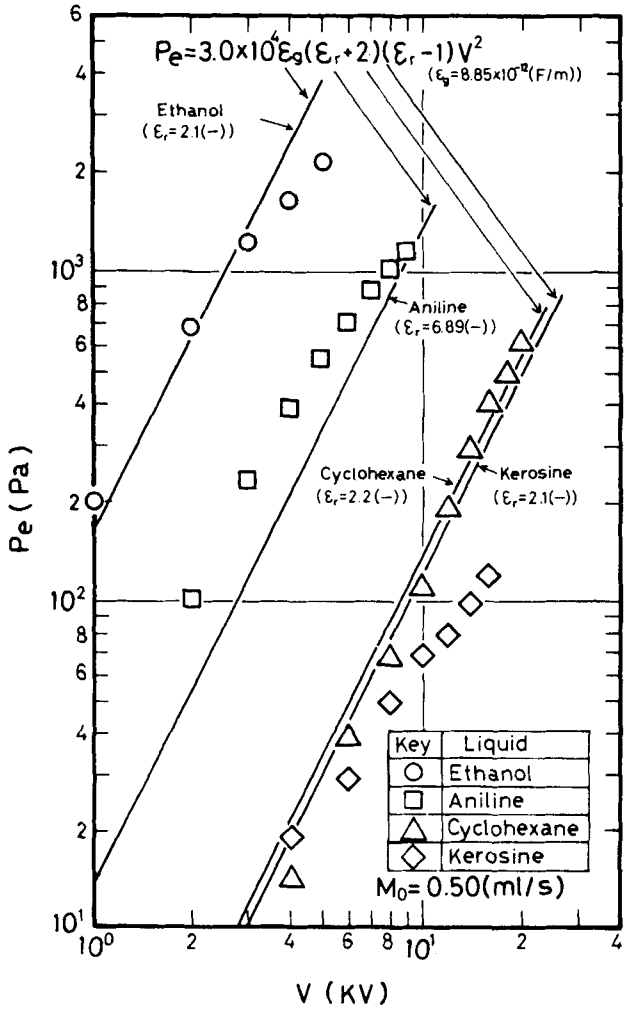

Figure 6. Relations between electric pressure at the end of the nozzle P_e and applied voltage V for various liquids for M_0 = 0.50 mL/s and L = 8 cm.

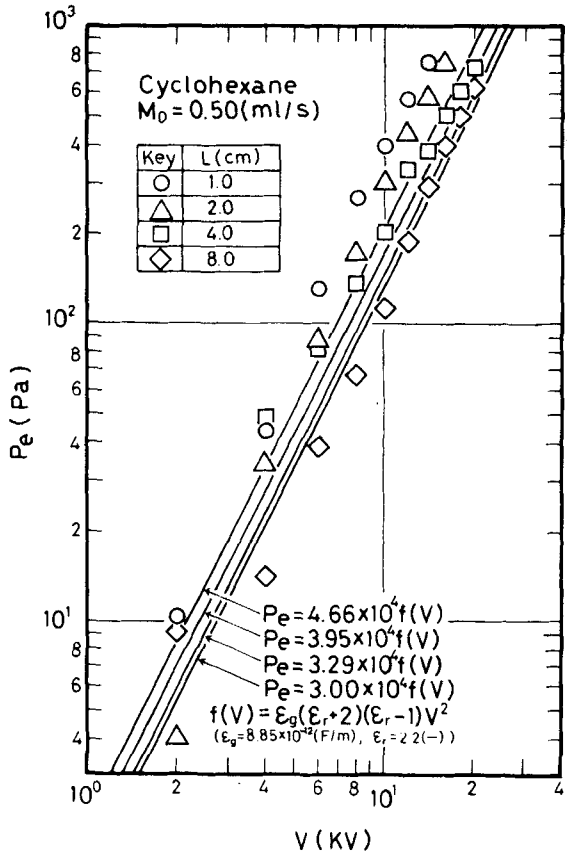

Figure 7. Relations between electric pressure at the end of the nozzle P_e and applied voltage V for various electrode gaps L for cyclohexane at M_0 = 0.50 mL/s.

The electric pressure buildup processes for imposed stepwise voltage is shown in Figure 8 for kerosine at 4 cm of electrode gap. Figure 8 and the observed results of the other liquids show that the transient response of pressure generation follow the approximation $P_{et}/P_e = 1 - e^{-t}/\tau$, where τ is the time constant and P_{et} is the transient electrical pressure. The time constants of approximated exponential decay model showed to be almost independent of the electrical relaxation time of liquid τ_e (= permittivity/conductivity). These larger time constants also shows no frequency effect of applied voltage when frequency is larger than 10^{-2} Hz.

Energy Efficiency

The energy efficiency η in current system can be defined as follows:

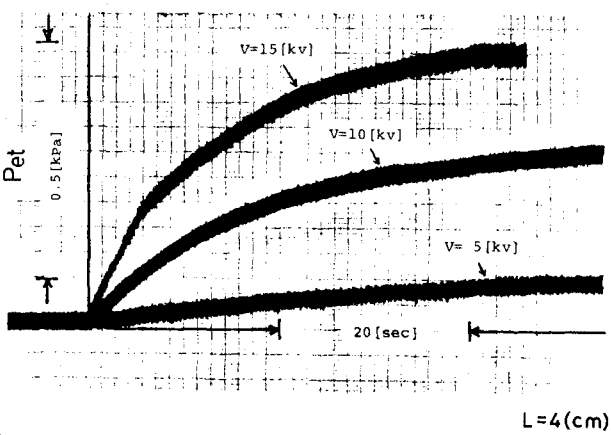

Figure 8. Electrical pressure generation processes for various imposed stepwise electric potential for kerosine at L = 4 cm.

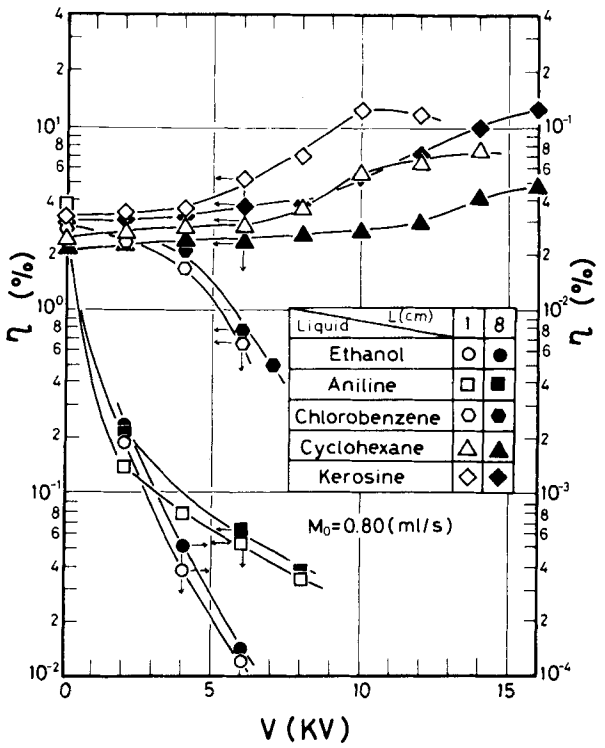

Figure 9. Relations between energy efficiency η and applied voltage V for various liquids and L at M_0 = 0.80 mL/s.

$$\eta = \frac{\text{consumed energy for surface enlargement}}{\text{total energy added to the system}} = \frac{6\sigma \cdot M/\bar{d}_B}{V \cdot i + P \cdot M} \times 100\,[\%] \qquad (10)$$

The first term of the denominator shows electrical energy, while the second is mechanical energy. Here we must note that $V \cdot i <$ PM for kerosene and cyclohexane and $V \cdot i \gg P \cdot M$ for other fluids

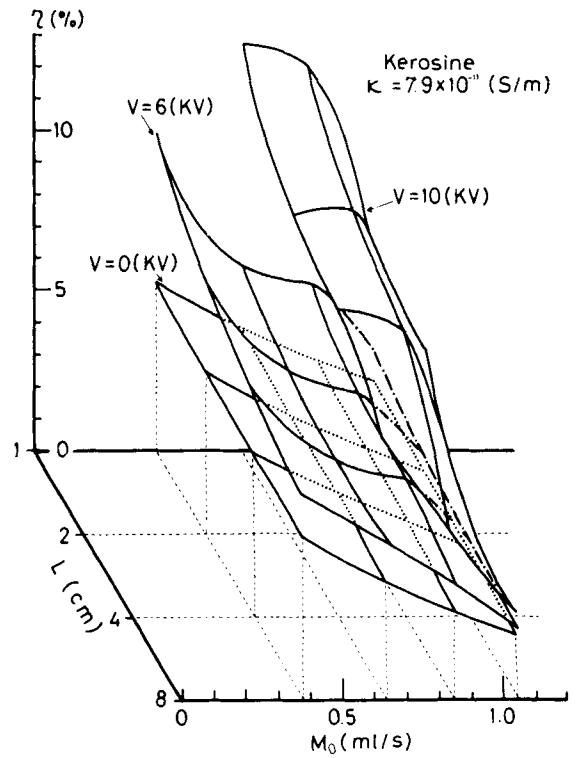

Figure 10. Three-dimensional picture of energy efficiency η for various applied voltage V, electrode gap L and gas flow rate M_0 for kerosine.

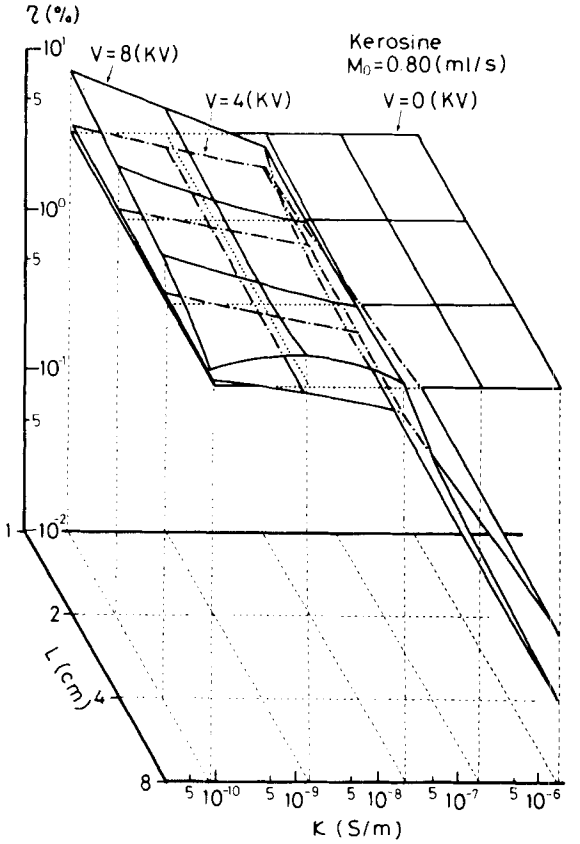

Figure 11. Three-dimensional picture of energy efficiency η for various applied voltage, V, conductivity κ and electrode gap L for kerosine/ASA-3 mixture.

as shown in Table 1. The average diameter $\bar{d}_B$ (Sauter mean diameter) is

$$\bar{d}_B = \sum_{i=1}^{N} d_{Bi}^3 \Big/ \sum_{i=1}^{N} d_{Bi}^2.$$

Typical average diameters are 2.5 and 0.5 mm for with and without electric field, respectively.

The relation between the efficiency and applied voltage for various liquids and electrode gap distances at gas flow rate M_o = 0.8 mL/s is shown in Figure 9. Figure 9 shows the relatively large dependence of the efficiency on the conductivity and permittivity. The figure also shows that the effect of gap distances is not always explicit. For nonpolar liquids such as kerosine and cyclohexane, higher efficiency was obtained for narrower gaps (L = 1 cm), while other liquids are opposite. The relationship between L, κ and M_o obtained from present experiments for kerosine are shown in Figure 10 for larger M_o and L. The effect of liquid conductivity on the η is shown in Figure 11 for various κ and L at M_o = 0.8 mL/s, where the conductivity of kerosine has been increased by adding an antistatic agent ASA-3 without changing its permittivity (Ogata andShinohara, 1977) in this experiment. The figure shows

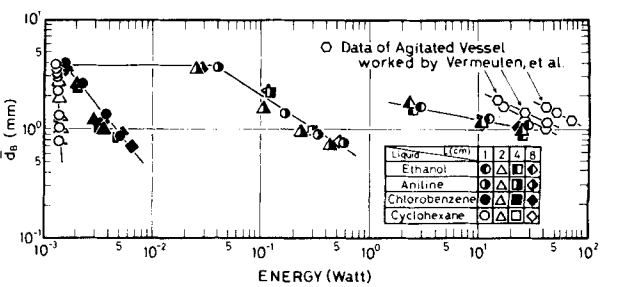

Figure 12. Variations of average bubble diameter $\bar{d}_B$ as a function of total energy for various liquids and L. The results of Vermeulen et al. are also plotted for comparison.

that the decrease of the efficiency is not so conspicuous up to 10^{-8} S/m. However, it becomes more pronounced when the conductivity is larger than 10^{-8} S/m. This might mean that the most part of electrical energy becomes consumed as Joule heating without contributing to bubble disruption for larger conductivity fluids.

The variations of the averaged bubble diameter $\bar{d}_B$ as a function of the total energy $(V \cdot i + P \cdot M)$ is shown for various liquid and L in Figure 12, where the data of stirred vessel for air-CCl_4 system by Vermeulen et al. (1955) are also plotted for comparison. The figure shows that effective bubble size reduction occurred in not only nonpolar liquids, but also in moderately polar liquid such as aniline. Moreover, the figure also shows that the energy needed for bubble size reductions in a kerosine and cyclohexane are over four orders of magnitude lower than those of stirred vessel, and even in ethanol, this value is still lower by a factor of five.

Rising Velocity of Bubbles

In order to understand the role of the EHD flow, the measurement of bubble rising velocity has been done. The superimposed strobo-pictures were taken from two flashed-back lights of known interval (2.4 ms) for bubble rising velocity determination. The vertical velocity component of rising bubbles was calculated from measuring the displacements of bubbles. It should be noted, however, that only the vertical component is valid here and that radial components cannot be obtained by such an approximated two-dimensional analysis (Ogata et al., 1981).

Figure 13 shows a normalized velocity u_e/u_c as a function of V for various liquids at 5 cm above the nozzle tip, where u_e is the averaged rising velocity, while u_c is the terminal bubble velocity and dependent of Reynold number (Bird et al., 1960).

$$u_c = \begin{cases} \dfrac{\rho g}{18\mu}\bar{d}_B^2 \text{ for } \mathrm{Re} < 2 \\ \left(\dfrac{2}{15}\right)^{2/3}(\rho g)^{2/3}(\mu\rho)^{-1/3}\bar{d}_B \text{ for } 2 < Re < 500 \end{cases} \quad (11)$$

Here, we must note that the values at $V = 0$ is slightly larger than unity caused by the unfully developed nature of u_e. However, it can be observed from Figure 13 that u_e/u_c becomes larger in proportion to applied electric field, permittivity and/or conductivity. For example, u_e of ethanol reaches to as much as three times of its terminal velocity at 3 kV. These enhanced velocities can be explained bubble acceleration due to the EHD flow as we analyzed in the earlier theoretical treatment. This enhancement increases with increasing permittivity as one also can observe in Figure 13. These phenomenon might mean that the larger part of electric energy would be still consumed in producing the EHD flow rather than Joule dissipations.

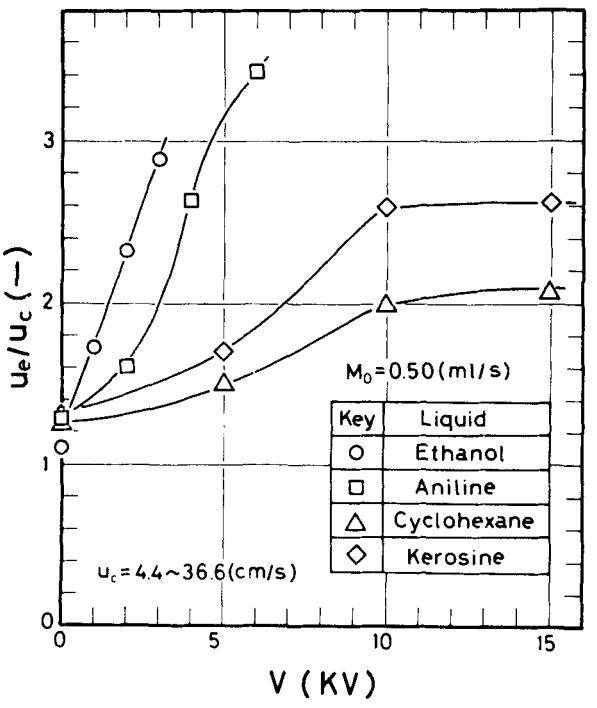

Figure 13. Relation between normalized rising velocity of bubbles u_e/u_c and applied voltage V for various liquids at M_0 = 0.50 mL/s at 5 cm above the nozzle tip.

ACKNOWLEDGMENT

We would like to express our sincere thanks to M. Akazaki, M. Hara, and K. Kojima for valuable discussions and comments. This work was supported partly by Natural Science and Engineering Council of Canada, and by McMaster University Science and Engineering Research Board (S. Ogata, J-S. Chang).

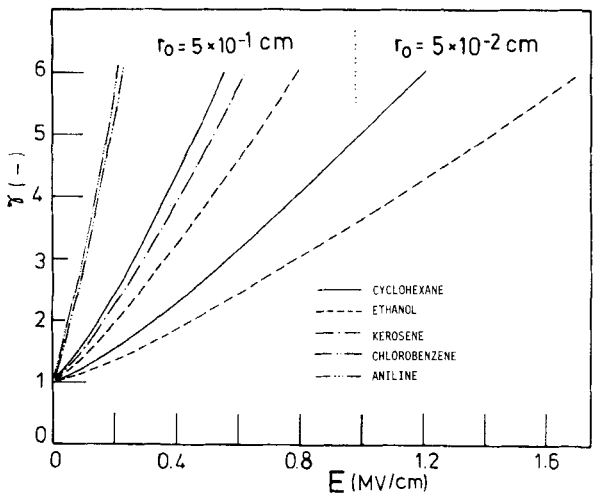

Figure A1. Elongation of gas bubbles in a uniform electric field for various fluids for $r_0 = 5 \times 10^{-2}$ and 5×10^{-1} cm.

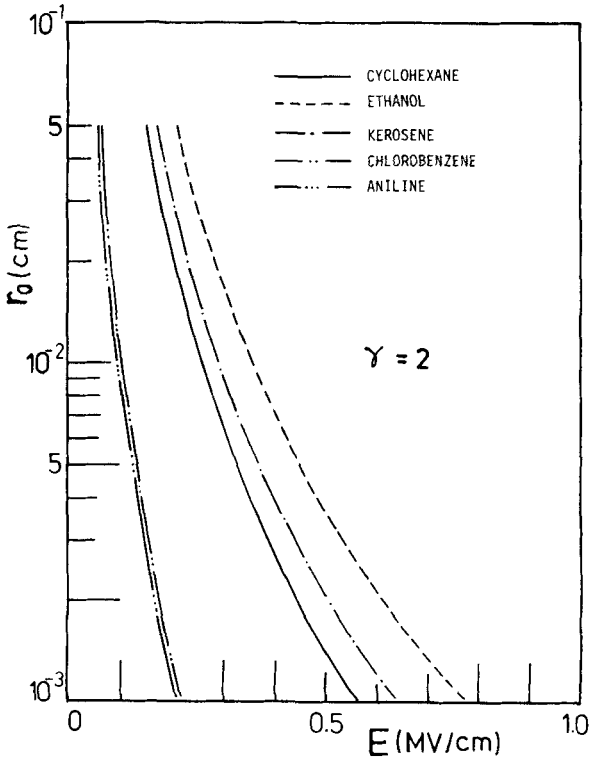

Figure A2. The effect of bubble sizes on the bubble elongation by a uniform electric field for various fluids at $\gamma = 2$.

APPENDIX I: ELONGATION OF BUBBLE DUE TO THE APPLIED ELECTRIC FIELD

Numerical $\gamma - E$ characteristic for present experimental fluid for $r_0 = 5 \times 10^{-1}$ and 5×10^{-2} cm are shown in Figure A1. Figure A1, together with Eq. 2 shows that the order of easier bubble disrupted fluids is aniline, chlorobenzene, cyclohexane, kerosine and ethanol when the electric field is relatively larger. This conclusion also agrees with the experiment (Ogata et al., 1980, Figure 7), except for smaller electric field, since Eq. 2 shows that the stability of the bubble is dependent upon both surface tension and interface electric field in this condition. Numerical $r_0 - E$ characteristics for the present experimental fluid for $\gamma = 2$ are shown in Figure A2. Figure A2 shows that the electric field needed to elongate bubble increases with decreasing bubble size. However, this difference is small for chlorobenzene and aniline, as shown in Figure A2 and the previous experiment (Ogata et al., 1980, Figure 7).

NOTATION

$d_B, \bar{d}B$ = bubble diameter and averaged one, respectively
E = local electric field
$\bar{E}, E_0$ = averaged electric field and nominal field strength V/L, respectively
F_o = constant dependent on bubble size
H = distance between bubble and grounded electrode
i = electric current
g = gravitational acceleration
L = distance between nozzle tip and grounded electrode
M, M_0 = gas flow rate with and without electric field
P, P_e = hydraulic pressure and electric pressure, respectively
r_0, R_2 = bubble radius without electric field
R_1 = nozzle radius
Re = Reynolds number
R_E = electric Reynolds number
S = total surface area of bubbles
u = velocity
V = applied voltage
z = vertical distance from grounded electrode

Greek Letters

γ = ratio of major to minor semiaxis
ψ = normalized electric field
ϕ, ϕ_c = electric potential and potential on conductor, respectively
ϵ = permittivity of fluids
η = energy efficiency
κ = conductivity of liquids
μ = viscosity of fluids
ρ = density of fluids
σ = surface tension
τ = relaxation time
ξ = wave height in gas-liquid interface
ζ = position in space

Subscripts

c = critical
e = electrical
g = gas
i = point i
int = interface
l = liquid
o = free space
1 = liquid
2 = gas
r = relative
z = vertical axis

LITERATURE CITED

Apfel'Baum, M. S., et al., "Electrical Convection in Dielectric Liquid," *Heat Transfer—Soviet Research*, **10**, 14 (1978).

Bird, R. B., W. E. Stewart and E. N. Lightfoot, *Transport Phenmomena*, John Wiley, New York, Chapter 6 (1960).

Brunner, K., and J. S. Chang, "Flow Regime Transitions under Electric Fields in a Horizontal Two-phase Flow," Conf. Record of IEEE IAS Meeting, 1042 (1980).

Chang, J. S., and F. Tran, "Numerical Analysis of Transient Natural Convection of Gas in Horizontal Cylindrical Annulus under DC Electric Field," "Natural Convection—HTD," I. Catton and R. N. Smith, Eds., ASME, New York, **16**, 51 (1981).

Garton, C. G., and Z. Krasucki, "Bubble in Insulating Liquids: Stability in an Electric Field," *Proc. Roy. Soc.*, London, **A280**, 211 (1964).

Kao, K. C., "Some Electromechanical Effects on Dielectrics," *Brit. J. Appl. Phys.*, **12**, 620 (1961).

Mashelkar, R. A., "Bubble Columns," *Brit. Chem. Eng.*, **15**(10), 1297 (1970).

Ogata, S., and H. Shinohara, "Electrical Properties of Liquids Adaptable to Electrostatic Atomization," *Kagaku Kogaku Ronbunshu*, **3**, 586 (1977).

Ogata, S., T. Yoshida, and H. Shinohara, "Small Air Bubble Formation in Insulating Liquids under Strong Nonuniform Electric Field," *Jpn. J. Appl. Phys.*, **18**, 411 (1979).

Ogata, S., K. Shigehara, T. Yoshida, and H. Shinohara, "Small Air Bubble Formation by Using Strong Nonuniform Electric Field," *IEEE Trans.*, **IAS, 16**, 766 (1980).

Ogata, S., M. Ishikawa, and T. Murakami, "Velocity Measurement of Electro-Statically Sprayed Droplets by Means of Two Laser Impulses of Different Wavelengths," *J. Elctrostatics*, **8**, 223 (1981).

Sato, M., M. Kuroda, and T. Sakai, "Effect of Electrostatics on Bubble Formation," *Kaguka Koguka Konbushu*, **5**, 380 (1979).

Shah, Y. T., B. G. Kelkar, S. P. Godbole, and W. D. Deckner, "Design Parameters Estimations of Buble Column Reactors," *AIChE J*, 3(3) 353 (1982).

Vermeulen, T., G. M. Williams, and G. E. Ianglois, "Interfacial Area in Liquid-Liquid and Gas-Liquid Agitation," *Chem Eng. Prog.*, **51**, 85-F (1955).

Zacky, A. A., and A. Nosseir, "Bubble Injection and Electrically Induced Hydrostatic Pressure in Insulating Liquids Subjected on Nonuniform Field," *J. Phys. D.: Appl. Phys.*, **10**, L 189 (1977).

Manuscript received December 17,1981; revision received September 16,1983 and accepted September 26, 1983.